Myeloid cell-specific deletion of AMPKα1 worsens ocular bacterial infection by skewing macrophage phenotypes

Authors: Sukhvinder Singh[1], Pawan Kumar Singh[2], Zeeshan Ahmad[1], Susmita Das[1], Marc Foretz[3], Benoit Viollet[3], Shailendra Giri[4], and Ashok Kumar[1,5 #]

Affiliations:

[1]Department of Ophthalmology, Visual and Anatomical Sciences, Kresge Eye Institute, Wayne State University School of Medicine, Detroit, MI, USA.

[2]Department of Ophthalmology/ Mason Eye Institute, University of Missouri School of Medicine, Columbia, MO, USA

[3]Université Paris cité, CNRS, Inserm, U1016, Institut Cochin, Paris 75014, France

[4]Department of Neurology, Henry Ford Health System, Detroit, MI, USA

[5]Department of Biochemistry, Microbiology, and Immunology, Wayne State University School of Medicine, Detroit, MI, USA.

 # Corresponding Author

Ashok Kumar, Ph.D.

Department of Ophthalmology, Visual, and Anatomical Sciences

Wayne State University School of Medicine

4717 St. Antoine, Detroit, MI 48201

Tel: (313) 577-6213; Fax: (313) 577-7781

E-mail: akuma@med.wayne.edu

Abstract

AMP-activated protein kinase (AMPK) plays a crucial role in governing essential cellular functions such as growth, proliferation, and survival. Previously, we observed increased vulnerability to bacterial (*S. aureus*) endophthalmitis in global AMPKα1 knockout (KO) mice. In this study, we investigated the specific involvement of AMPKα1 in myeloid cells using $LysM^{Cre}$; $AMPK\alpha1^{fl}$ mice. Our findings revealed that while endophthalmitis resolved in wild-type (WT) B6 mice, the severity of the disease progressively worsened in AMPKα1 deficient mice over time. Moreover, the intraocular bacterial load and inflammatory mediators (e.g., IL-1β, TNF-α, IL-6, and CXCL2) were markedly elevated in the $LysM^{Cre}$; $AMPK\alpha1^{fl}$ mice. Mechanistically, the deletion of AMPKα1 in myeloid cells skewed macrophage polarization toward the inflammatory M1 phenotype and impaired the phagocytic clearance of *S. aureus* by macrophages. Notably, transferring AMPK-competent bone marrow from wild-type mice to AMPKα1 KO mice preserved retinal function and mitigated the severity of endophthalmitis. Overall, our study underscores the role of myeloid-specific AMPKα1 in promoting the resolution of inflammation in the eye during bacterial infection. Hence, therapeutic strategies aimed at restoring or enhancing AMPKα1 activity could improve visual outcomes in endophthalmitis and other ocular infections.

Keywords: Eye, Endophthalmitis, *S. aureus*, Inflammation, AMPK, Immunometabolism, macrophages

Introduction

Bacterial endophthalmitis is a serious eye infection that can lead to vision loss due to severe intraocular inflammation and tissue damage [1-4]. Staphylococci, especially *Staphylococcus (S) aureus*, are the primary culprits, and although they account for only 10-15% of cases, they often lead to poor outcomes [5]. Typically, during ocular surgeries, *S. aureus* gains entry into the eye, releasing virulence factors such as toxins and cell wall components such as peptidoglycan and lipoteichoic acids [6]. Host immune cells recognize these bacterial elements through pattern recognition receptors and trigger a complex inflammatory immune response [3, 7]. Moreover, the blood-retinal barrier, which is crucial for ocular defense, becomes compromised, allowing a large influx of immune cells, predominantly neutrophils and monocytes/macrophages, into the vitreous chamber [8, 9]. While this influx is necessary to combat bacterial growth, it also leads to excessive inflammation, which, if unchecked, damages intraocular tissues, especially the neurosensory retina, resulting in irreversible vision loss [2, 6, 10]. Unfortunately, there is no standardized treatment to control intraocular inflammation, and visual outcomes often remain suboptimal even after aggressive antibiotic treatments and vitrectomy surgeries [11, 12]. Moreover, the increase in antibiotic-resistant ocular pathogens poses a significant challenge in managing these infections [13, 14]. Therefore, research aimed at understanding the mechanisms governing inflammation initiation and resolution holds promise for identifying potential therapeutic targets to prevent and treat bacterial endophthalmitis.

Given the intricate nature of host-pathogen interactions, we employed an integrated approach combining metabolomics and transcriptome analysis of *S. aureus*-

infected retina tissues to identify novel immunomodulatory and antimicrobial targets [15-17]. Our findings revealed significant impacts on various pathways during endophthalmitis, including inflammatory and immune responses, antimicrobial defense mechanisms against bacteria, endoplasmic stress, cell trafficking, and death, as well as energy metabolism, notably involving disruptions in NAD+ and lipid biosynthesis [1, 15, 16, 18]. Within the realm of energy metabolism, AMP-activated protein kinase (AMPK) has emerged as a key player in maintaining host energy balance [19]. AMPK not only governs cellular energy metabolism but also regulates immune responses by modulating immune signaling pathways [20-22]. This cross-talk between AMPK and immune signaling pathways has crucial implications for reshaping the metabolic and functional profiles of immune cells [23, 24].

In our previous work, we demonstrated that both genetic (using AMPKα1 global knockout mice) and pharmacological (with AICAR) activation of AMPK confer protection against endophthalmitis [1]. However, a limitation of this study was the inability to discern the cell-specific contribution of AMPK to the pathogenesis of bacterial endophthalmitis. Given that the primary immune cells involved in endophthalmitis are of myeloid origin, we aimed to investigate the specific role of AMPKα1 in myeloid cells during endophthalmitis. In this study, employing myeloid-specific AMPKα1 knockout mice ($LysM^{Cre}$; $AMPK\ \alpha1^{fl}$) and bone marrow reconstitution chimera approaches, we found that the loss of AMPKα1 in myeloid cells worsens bacterial endophthalmitis highlighting the importance of myeloid-specific AMPK in bacterial endophthalmitis.

Materials and Methods

Mice and ethical statement

B6.SJL-Ptprca Pepcb/BoyJ (Pep Boy) mice were obtained from the Jackson Laboratory (Bar Harbor, ME), while wild-type (WT) and AMPKα1 global knockout (KO) (B6/129 background) were used as described [1]. AMPKα1^{fl} mice were purchased from Jackson laboratory (#014141) and crossed with LysM^{Cre} (#004781) to generate a myeloid-specific loss of AMPKα1 referred to as LysM^{Cre}; AMPKα1^{fl}. Six- to eight-week-old mice of both male and female sex were utilized. They were housed in a controlled-access Division of Laboratory Animal Resources (DLAR) facility at the Kresge Eye Institute, maintained under a 12-hour light/12-hour dark cycle at a temperature of 22°C, and provided ad libitum access to water and LabDiet rodent chow (PicoLab; LabDiet, St. Louis, MO). All procedures were conducted per the Association for Research in Vision and Ophthalmology (ARVO) Statement for the Use of Animals in Ophthalmic and Vision Research and were approved by the Institutional Animal Care and Use Committee (IACUC) of Wayne State University (protocol # IACUC-22-04-4557).

Bacterial strain and induction of endophthalmitis

The *S. aureus* strain RN6390 was cultured in tryptic soy broth and on agar plates (TSB/TSA; Sigma-Aldrich, St. Louis, MO). Bacterial endophthalmitis was induced in mice, as described previously [3, 25]. Briefly, mice were anesthetized and intravitreally injected with *S. aureus* (500 CFU/eye) using a 34G needle under a dissecting microscope within a biosafety cabinet. Contralateral eyes received sterile PBS injections and served as controls. Disease progression was monitored through slit lamp examination and other modalities. Scotopic electroretinography (ERG) was used to determine retinal function using the Celeries ERG system (Diagnosis LLC, Lowell, MA),

as per the manufacturer's recommendation and standardized in our prior studies [16, 26].

Isolation of bone marrow-derived macrophages (BMDMs)

Mouse bone marrow-derived macrophages (BMDMs) were isolated according to previously established protocols [27]. Briefly, mice were euthanized, and bone marrow was flushed from the tibias and femurs using RPMI media supplemented with 10% FBS and 0.2 mM EDTA. The cells were then centrifuged at 400xg for 5 minutes at 4°C to pellet them. Red blood cells (RBCs) were lysed by adding 0.2% NaCl (hypotonic) solution for 20 seconds, followed by the addition of 1.6% NaCl (hypertonic) and subsequent centrifugation. The cell pellets were rinsed with RPMI media, re-suspended, seeded in RPMI media supplemented with 10% FBS, 100 U/ml penicillin, 100 mg/mL streptomycin, and 10 ng/ml M-CSF for macrophage differentiation and cultured at 37°C in 5% CO2. Six days post-differentiation, BMDMs were seeded at a concentration of 4×10^6 cells/mL in 60 mm Petri dishes for *in vitro* experiments.

Bacterial burden estimation

The eyes were enucleated following *S. aureus* infection at 24 h, 48 h, and 72 h post-infection. Whole-eye lysates were prepared in 250 µL of PBS by beating with stainless steel beads in a tissue lyser (Qiagen, Valencia, CA). A 50 µL aliquot of the tissue homogenate was serially diluted and plated on Tryptic Soy Agar (TSA) to quantify the viable bacterial load. The colonies were counted the next day, and the results are reported as the mean number of CFU/eye.

Cytokine ELISA

For *in-vivo* samples, eyes were enucleated, and lysates were prepared using a tissue lyser as described above. The tissue homogenates were then centrifuged at 10,000 x g for 20 minutes at 4°C, and the resulting supernatant was utilized for cytokine estimation. In the *in vitro* studies, conditioned media from both the *S. aureus*-infected and drug-treated groups, as well as the vehicle control group, were collected and preserved for cytokine measurements. Mouse ELISA was conducted to quantify the inflammatory cytokines IL-1β, IL-6, TNF-α, and CXCL2 according to the manufacturer's instructions (R&D Systems, Minneapolis, USA).

Histological analysis

The eyes were enucleated and preserved in modified Davidson's fixative for subsequent histopathological analysis. The embedding, sectioning, and staining with hematoxylin & eosin (H&E) were carried out by Excalibur Pathology, Inc. (Oklahoma City, OK, USA).

RNA extraction and qPCR analysis

Total RNA was extracted from both the neural retina and BMDMs using TRIzol according to the manufacturer's guidelines (Thermo Scientific, Rockford, IL). Subsequently, the RNA was reverse transcribed using a Maxima first-strand cDNA synthesis kit following the manufacturer's protocol (Thermo Scientific, Rockford, IL). Quantitative assessment of gene expression was conducted via SYBR green-based qPCR, employing gene-specific primers, on the Step One Plus Real-Time PCR System (Applied Biosystems, Foster City, CA, USA). Data analysis was performed utilizing the comparative $^{\Delta\Delta}$Ct method, as previously described [28]. The expression levels of genes in the test samples were normalized to endogenous β-actin controls.

Bacterial phagocytosis assay

BMDM cells (10^6 cells/dish) were cultured in 60 mm Petri dishes in RPMI-1640 media. Subsequently, the cells were exposed to *S. aureus* at an MOI of 10:1 for 2 hours. After the incubation period, the cells were washed and treated with gentamicin (200 μg/mL) for 2 hours to eliminate extracellular bacteria. The absence of extracellular bacteria was confirmed through dilution plating and enumeration of CFUs. Two hours post-gentamicin treatment, the cells were washed with RPMI-1640 and incubated with fresh media containing gentamicin (200 μg/mL) for 1, 3, or 6 hours. To quantify internalized bacteria, following the designated incubation periods, the cells were washed three times with PBS and lysed using 0.01% Triton X-100. The lysed cells were collected by scraping and centrifuged at 7500 x g for 5 minutes. The resulting cell pellets were washed twice with PBS through centrifugation at 7500 x g for 5 minutes each time. The pellets were then resuspended in 1 mL sterile PBS, serially diluted, and plated onto TSA plates for enumeration of bacterial counts.

Immunostaining

BMDMs were cultured in a four-well chamber slide (Fisher Scientific, Rochester, NY). Following treatment, the cells were infected with *S. aureus* at an MOI of 10:1 for 3 hours. At the specified time points, the infected cells were fixed with 4% PFA in PBS at 4°C. After washing with PBS, the cells were permeabilized and blocked with 1% (w/v) BSA and 0.4% Triton X-100 in PBS for 1 hour at room temperature (RT). Subsequently, the cells were incubated overnight at 4°C with primary antibodies against iNOS and Arg1 (1:100 dilution, Cell Signaling Technology, Danvers, MA). Following the removal of the primary antibodies, the cells were thoroughly washed with PBS and then incubated

with anti-mouse/rabbit Alexa Fluor 485/594-conjugated secondary antibodies (1:200 dilution) for 1 hour at RT. Finally, the cells were washed four times (5 minutes each) with PBS, and the slides were mounted in Vectashield antifade mounting medium containing DAPI (Vector Laboratories, Burlingame, CA) before visualization using a Keyence microscope (Keyence, Itasca, IL).

Western blotting

Protein samples were obtained by directly lysing cells in radioimmunoprecipitation assay (RIPA) buffer containing protease and phosphatase inhibitor cocktails. The total protein concentration of the cell lysates was determined using a Micro BCA™ protein assay kit (Thermo Scientific, Rockford, IL). Subsequently, protein samples (30-40 µg) were separated via SDS–PAGE (8% or 12%) and transferred onto a nitrocellulose membrane (0.45 µm) using a wet transfer system. The membranes were then blocked in 5% (w/v) dry milk in Tris-buffered saline with Tween (TBST) for 1 hour at room temperature. Following blocking, the membranes were incubated with primary antibodies against iNOS, Arg1, and HSP-90 (Cell Signaling Technology, Danvers, MA) according to the manufacturer's instructions, followed by incubation with appropriate horseradish peroxidase-conjugated secondary antibodies. After four TBST washes, the membranes were exposed to SuperSignal West Femto chemiluminescent substrate and imaged using an iBright fluorescence imager (Thermo Scientific, Rockford, IL). Densitometry analysis was carried out using ImageJ software (Rasband, W.S., ImageJ, U.S. National Institutes of Health, Bethesda, Maryland)

Flow cytometry

Flow cytometry was conducted following previously established methods to assess the adoptive transfer and infiltration of neutrophils into the eyes [3]. In brief, retinas from euthanized mice were isolated and digested with Accumax (Millipore) for 10 minutes at 37°C. A single-cell suspension was generated by gently triturating the cell mixture with a 22G needle and subsequently passing it through a 40-μm cell strainer (BD Falcon, San Jose, CA, USA). The cells were then blocked using Fc Block (BD Biosciences) for 30 minutes, followed by three washes with PBS containing 1% bovine serum albumin (BSA). Subsequently, the cells were stained by incubating them with CD45.1-APC, CD45.2-PE, and Ly6G-FITC conjugated antibodies (BD Biosciences) on ice for 20 minutes in the dark. After incubation, the cells were washed and suspended in PBS supplemented with 1% BSA. Flow cytometric analysis was performed using an Accuri C6 flow cytometer and accompanying software (BD Biosciences), data analysis was conducted using FlowJo™ v8 Software (BD Life Sciences).

Bone marrow chimera

The adoptive transfer of naïve bone marrow cells into AMPKα1 KO mice (with the CD45.2 allele) and B6. SJL-Ptprca Pepcb/BoyJ (Pep Boy, used as wild-type mice with the CD45.1 allele) was carried out via the busulfan method [29]. Initially, recipient mice received a single preconditioning dose of 20 mg/kg busulfan (Cayman Chemicals, Ann Arbor, MI) intraperitoneally daily until a cumulative dose of 100 mg/kg was achieved. Subsequently, all mice were intravenously injected with $1x10^7$ donor bone marrow cells obtained from the recipient mouse via tail vein injection in 200 μL of phosphate-buffered saline (PBS). Starting at 2 weeks after transplantation, approximately 20-30 μL of blood was collected from the lateral saphenous vein, and CD45.1 vs CD45.2 expression was

assessed in peripheral blood using flow cytometry. Efficient engraftment of donor bone marrow (>80%) was observed at 6 weeks post-transplantation. Following successful engraftment, the mice were subjected to endophthalmitis as described above.

RNA sequencing

For RNA sequencing, total RNA was extracted from the BMDMs of the AMPKα1 KO and WT mice in biological triplicates using RNeasy Mini Kits (Qiagen, Hilden, Germany). The sequencing procedures were conducted by Novogene Co., Ltd. RNA sequencing (RNA-seq) libraries were constructed from high-quality RNA using NEBNext Ultra™ II RNA Library Prep kits (New England BioLabs, Ipswich, MA, USA) following the manufacturer's instructions. Sequencing was performed on the NovaSeq 6000 platform as paired-end 150-bp reads (Illumina), with a sequencing depth of approximately 30 million reads per sample. Differential gene expression analyses were conducted using DESeq2, while GO enrichment analysis was carried out using PANTHER and KEGG pathways analyses.

Statistical Analysis

Statistical analyses were conducted using Prism version 9.2 (GraphPad, San Diego, CA). Group comparisons were assessed using one-way ANOVA followed by Tukey's Multiple Comparison post-hoc tests, and data were presented as mean ± SD. A confidence interval of 95% was applied for all statistical tests. A p-value of <0.05 was considered statistically significant. Unless specified otherwise, all experiments were performed at least three times.

Results

Myeloid-specific AMPKα1 deficiency exacerbated bacterial endophthalmitis

The hallmark of bacterial endophthalmitis is the infiltration of myeloid cells such as neutrophils and monocytes into the eye [6]. To investigate the role of AMPK in these cells during ocular infections, we induced *S. aureus* endophthalmitis in both AMPK $\alpha1^{fl}$ (Wt) and $LysM^{Cre}$; $AMPK\alpha1^{fl}$ mice using a low-dose infection model, in which 500 colony-forming units (CFUs) of *S. aureus* were administered. Although this dosage resolved in wild-type mice, it led to severe endophthalmitis in $LysM^{Cre}$; $AMPK\alpha1^{fl}$ mice [3, 16]. We monitored the progression of endophthalmitis through daily eye exams, retinal function testing, histopathological analysis, and estimation of intraocular bacterial burden and inflammation. Compared to $AMPK\alpha1^{fl}$ mice, endophthalmitis worsened in $LysM^{Cre}$; $AMPK\alpha1^{fl}$ mice, indicated by a time-dependent increase in corneal haze, opacity, and hypopyon formation (**Fig. 1A**). Histopathological analysis revealed increased retinal folding, tissue disintegration, and significant cellular infiltrates in the vitreous chamber of $LysM^{Cre}$; $AMPK\alpha1^{fl}$ mouse eyes (**Fig. 1B**). Electroretinography (ERG) demonstrated a notable decrease in both a- and b-wave amplitudes in $LysM^{Cre}$; $AMPK\alpha1^{fl}$ eyes at various time points (**Fig. 1C**). Additionally, the bacterial burden was relatively greater in $LysM^{Cre}$; $AMPK\alpha1^{fl}$ mice (**Fig. 1D**). Overall, a greater percentage of eyes exhibited damage due to *S. aureus* endophthalmitis in $LysM^{Cre}$; $AMPK\alpha1^{fl}$ mice compared to $AMPK\alpha1^{fl}$ (**Fig. 1E**).

Furthermore, in addition to direct retinal damage caused by bacterial toxins, uncontrolled inflammation resulting from excessive infiltration and activation of innate immune cells such as neutrophils contributes to bystander tissue damage. To evaluate intraocular inflammation, we analyzed the expression of inflammatory cytokines at both

the mRNA (**Fig. 2A**) and protein (**Fig. 2B**) levels at various time points. Notably, myeloid-specific deletion of AMPKα1 led to higher expression of inflammatory cytokines. For instance, the transcript levels of *Il-6* and *Cxcl2* were elevated at 72 hours, while the protein levels increased at both 48 and 72 hours. Conversely, AMPKα1-deficient macrophages exhibited consistently increased transcript levels of the inflammatory cytokines *IL-1β* and *TNF-α* at all time points, with protein levels peaking at 48 or 72 hours. Additionally, we investigated the inflammatory response of bone marrow-derived macrophages (BMDMs) from both AMPKα1^{fl} and LysM^{Cre}; AMPKα1^{fl} mice, revealing increased levels of inflammatory mediators in AMPKα1 KO BMDMs consistent with the *in vivo* data (**Fig. S1**). Taken together, these findings suggest that AMPKα1 deficiency in myeloid cells enhances inflammation and exacerbates endophthalmitis.

AMPKα1 deficient BMDMs exhibit distinct transcriptomic profiles

To elucidate the mechanisms underlying the heightened inflammatory response of *S. aureus*-infected AMPKα1-deficient mice, we performed RNA-seq analysis. This analysis revealed ~3,516 differentially expressed genes (DEGs) in *S. aureus*-infected AMPKα1 KO BMDMs compared to Wt, with 1,665 genes showing upregulation and 1,848 displaying downregulation (**Fig. 3A**). Gene set enrichment analysis indicated significant alterations in pathways associated with inflammation, metabolism, endoplasmic reticulum stress, and cholesterol biosynthesis, with notable downregulation of bacterial defense pathways in AMPKα1-deficient macrophages (**Fig. 3B**). Further analysis of DEGs based on the encoded proteins corroborated these findings, i.e., a reduction in pathways related to inflammation resolution and responses to lipopolysaccharide and bacteria (**Fig. 3C**). A heat map was constructed to visualize the

highly downregulated and upregulated genes involved in inflammatory and antimicrobial immune defense (**Fig. 3D**).

Given the increased bacterial burden observed in *S. aureus*-infected LysM^{Cre}; AMPKα1^{fl} mice, we hypothesized that this might stem from the downregulation of antimicrobial genes such as *S100a7*, *a8*, and *a10* in the RNAseq data. To verify this, we examined their expression via qPCR and found that their levels were significantly lower in AMPKα1 KO BMDMs (**Fig. S2A**). Consistently, AMPKα1 KO BMDMs exhibited reduced intracellular phagocytic killing of *S. aureus* in the gentamicin protection assay (**Fig. S2B**). Collectively, these findings underscore the role of AMPKα1 in regulating antibacterial activity by enhancing phagocytic killing and the induction of antimicrobial molecules during bacterial infection.

AMPKα1 deficiency promotes the M1 milieu during S. aureus endophthalmitis

Our RNAseq analysis revealed that a diminished response to bacterial infection corresponds with the exacerbated endophthalmitis observed in AMPKα1-deficient mice. Given the pivotal role of macrophages in inflammation resolution *via* the transition from a pro-inflammatory (M1) to an anti-inflammatory (M2) phenotype, we examined the expression of these markers in infected retinal tissue and cultured BMDMs. Our data demonstrated relatively higher transcript levels of the classical M1 markers *Cox2*, *iNos*, and *Il23*, in the retinas of LysM^{Cre}; AMPKα1^{fl} mice compared to Wt mice (**Fig. 4A**). Conversely, the levels of M2 phenotype markers (*Arg1*, *Fizz1*, and *Yam1/2*) were downregulated in LysM^{Cre}; AMPKα1^{fl} mice retinas. To corroborate these findings, we assessed the pro-inflammatory (M1) and anti-inflammatory (M2) signatures in BMDMs isolated from LysM^{Cre}; AMPKα1^{fl} and AMPK^{fl} mice, challenging them with *S. aureus*.

Immunostaining of *S. aureus*-infected LysM^{Cre}; AMPKα1^{fl} macrophages revealed increased levels of iNos (**Fig. 4C**) and decreased expression of Arg1 (**Fig. 4D**). Similarly, western blot analysis also demonstrated increased protein levels of iNos (**Fig. 4E&F**) and decreased Arg1 levels (**Fig. 4G&H**) in AMPKα1-deficient macrophages. These results further support the notion that AMPKα1 regulates the balance between the M1 and M2 phenotypes, whereby its deficiency promotes the inflammatory phenotype in the eye.

Bone marrow reconstitution of AMPKα1-deficient mice ameliorated endophthalmitis

To illustrate the protective function of myeloid AMPKα1 during endophthalmitis, we used a bone marrow chimera approach, in which bone marrow from donor PepBoy mice (CD45.1 allele) were transferred to recipient AMPKα1-deficient mice (CD45.2 allele) (Wt > KO) and vice versa (KO > Wt) (**Fig. 5A- schematic**). This adoptive transfer yielded greater than 80% efficiency of bone marrow transfer in the recipient mice. Once stable bone marrow chimeras were established, *S. aureus* endophthalmitis was induced, and a time-course study was conducted. Eye imaging revealed decreased opacity and corneal haze in the bone marrow of AMPKα1 KO mice with Wt (PepBoy) bone marrow compared to those with AMPKα1 KO bone marrow in Wt mice (**Fig. 5B**). Electroretinography analysis demonstrated better retention of a- and b-wave amplitudes in AMPKα1 KO mice with Wt bone marrow (**Fig. 5C**). Furthermore, transfer of Wt chimera in AMPKα1 KO mice mitigated disease severity, as evidenced by decreased corneal opacity (**Fig. 5D**) and reduced intraocular bacterial burden (**Fig. 5E**).

Subsequently, we assessed intraocular inflammation and found that Wt > KO chimera exhibited significantly lower levels of inflammatory markers such as IL-1β, IL-6, TNF-α, and CXCL2 (**Fig. 5F**). This reduction correlated with a decrease in neutrophil infiltration in AMPKα1 KO chimera (**Fig. 5G)** compared to PepBoy mice with AMPKα1-deficient bone marrow (**Fig. 5H**). Thus, myeloid-specific AMPKα1 contributes to inflammation resolution and mitigates bacterial endophthalmitis.

Discussion

Bacterial endophthalmitis remains the most common vision-threatening complication of eye surgeries and ocular trauma [4]. Owing to the rapid progression and poor prognosis of endophthalmitis, early treatments with intravitreal injections of empirical antibiotics remain the main treatment option for bacterial endophthalmitis [30]. Antibiotics, while destroying bacteria, may release lipopolysaccharides [31, 32] lipoteichoic acid, and peptidoglycan from bacterial cell walls, including that of *S. aureus* (*SA)*[32], and evoke an inflammatory response [2, 33]. To suppress inflammation, intravitreal injections of corticosteroids are recommended, but the usage of steroids along with antibiotics for endophthalmitis has been marred with controversial outcomes in humans [34-38] and animal studies [39-43]. Moreover, steroid-related side effects, including elevated intraocular pressure (IOP), cataract formation, and retinal detachment, further hamper their inclusion in the management of endophthalmitis [44]. Thus, there is an urgent need to develop non-immunosuppressive anti-inflammatory therapies. In this study, we demonstrated an anti-inflammatory and protective role of myeloid-specific AMPK in bacterial endophthalmitis.

AMPK is an evolutionarily conserved heterotrimeric kinase with α, β, and γ subunits that primarily regulate cellular energy homeostasis [23]. The AMPK complex is activated either by increases in cellular AMP or ADP or by phosphorylation on Thr172 by upstream kinases, such as CaMKK-β, LKB1, or TAK1 [45-50]. This enhanced activity, in turn, controls signaling pathways that regulate protein synthesis, cell division, and intracellular membrane trafficking. Recent studies on AMPK regulation indicate that it not only functions as an intracellular energy sensor but also functions as a stress sensor to maintain intracellular homeostasis during infectious, autoimmune diseases and skeleton muscle regeneration [51-53]. Previously, using global AMPKα1 KO mice, we reported that loss of AMPKα1 increased the severity of bacterial endophthalmitis. However, the cell-specific role of AMPKα1 was not determined. Here, our data showed that myeloid cell-specific AMPKα1 plays a protective role during endophthalmitis as evidenced by worse disease outcomes in $LysM^{Cre}$; $AMPK\alpha1^{fl}$ mice (**Fig. 6**). Moreover, the protective effects of AMPKα1 on myeloid cells are exhibited via several potential mechanisms.

Here, we observed that the bacterial burden was greater in myeloid-specific AMPKα1 deficient mice. As we reported that activation of AMPKα and its downstream ACC in retinal Müller glia regulate autophagy-mediated clearance of *S. aureus* [17], we hypothesized that lack of AMPKα will impair pathogen clearance. Notably, phagocytosis of the pathogen activates the host autophagy initiation complex and the upstream regulatory components LKB1 and AMPKα1, which regulate autophagy induction through their kinase activities [54]. Deletion of AMPKα1 in myeloid cells results in susceptibility to exacerbated bacterial infection and host tissue cell death. In support of these

findings, our data showed that BMDMs from LysM^{Cre}; AMPKα1^{fl} mice had reduced phagocytic killing of *S. aureus*. Moreover, AMPKα1 deficiency led to a significant decrease in the bacterial infection-induced expression of antimicrobial peptides which might also contribute to greater bacterial burden in the eyes. Our results corroborate previous studies reporting the increased phagocytic activity (*E. Coli* and *L. pneumophila*) of macrophages upon pharmacological activation of AMPK *via* AICAR or metformin treatment [55, 56]. Moreover, the defect in phagocytosis following AMPKα1 ablation in macrophages is associated with their inability to undergo phenotypic transition, explaining the defect in bacterial clearance. A recent study has shown that restoring AMPK activity accelerates recovery from bacterial pneumonia [57]. Similarly, we also reported that AMPK activation inhibits viral replication in retinal cells [58]. These studies highlight the multifaceted roles of AMPK in viral and bacterial infections [59] through the regulation of cellular metabolism [60, 61].

Macrophages are also highly plastic innate immune cells, and environmental stimuli or bacterial infection can generate macrophages with a range of different phenotypes and functions [62]. The classical activation of macrophages generates M1 macrophages with pro-inflammatory properties, while alternative activation generates M2 macrophages with anti-inflammatory properties [63]. M1 macrophages exacerbate tissue injury whereas M2 macrophages promote the resolution of inflammation upon tissue injury [63, 64]. A careful examination of LysM^{Cre}; AMPKα1^{fl} revealed impaired inflammation resolution, leading to a subtle but significant increase in the expression of M1 macrophage phenotype markers (*iNos* and *Il23* expression) with the endophthalmitis progression. In contrast, the same mice showed a decrease in M2 macrophage

phenotype markers (*Arg1* and *Fizz1*), corresponding to an anti-inflammatory state, resulting in accelerated inflammation and endophthalmitis. Interestingly, a previous study showed that AMPKα1 mediated the regulation of macrophage skewing at the time of inflammation resolution during skeletal muscle regeneration [53]. Our data showing higher levels of inflammatory mediators in $LysM^{Cre}$; $AMPK\alpha1^{fl}$ mice eyes indicate the predominance of the M1 milieu which results in inflammation mediated retinal tissue damage.

To further confirm the role of AMPKα1 in ocular infection, we generated bone-marrow chimeras and showed the ability of AMPKα1-competent bone marrow-derived cells to rescue AMPKα1 KO from severe endophthalmitis. Consequently, impaired inflammation resolution was observed in KO -> Wt chimera where Wt macrophages were replaced with macrophages lacking AMPKα1 expression, whereas a benefit was observed in Wt -> KO chimera expressing AMPKα1 in macrophage. Moreover, the extent of endophthalmitis resolution in the AMPKα1 KO recipients was similar to those in Wt mice. This indicated that AMPKα1 expressed in infiltrating/residential myeloid cells contributes to endophthalmitis resolution.

In summary, our study demonstrated the protective role of myeloid cell-specific AMPKα1 during bacterial endophthalmitis. These effects are mediated by enhanced phagocytic clearance of bacteria and the promotion of inflammation resolution via inducing M2 macrophage phenotype. Therefore, AMPKα1 activation can be targeted therapeutically to treat bacterial endophthalmitis.

Acknowledgments

This study was supported by National Institute of Health grants R01EY026964, R01EY027381, R21AI140033 (AK), and an unrestricted grant from Research to Prevent Blindness (RPB) to the Department of Ophthalmology, Visual, and Anatomical Sciences supported this study. The immunology resource core is supported by NIH center grant P30EY004068. The authors are also grateful to other lab members for their helpful discussion and editing of the final manuscript. The funders had no role in study design, data collection, interpretation, or the decision to submit the work for publication.

Conflict of Interest.

The authors declare no competing interests.

Data availability

All data are contained within the article.

References

1. Kumar, A., S. Giri, and A. Kumar, *5-Aminoimidazole-4-carboxamide ribonucleoside-mediated adenosine monophosphate-activated protein kinase activation induces protective innate responses in bacterial endophthalmitis.* Cell Microbiol, 2016. **18**(12): p. 1815-1830.
2. Kumar, A. and A. Kumar, *Role of Staphylococcus aureus Virulence Factors in Inducing Inflammation and Vascular Permeability in a Mouse Model of Bacterial Endophthalmitis.* PLoS One, 2015. **10**(6): p. e0128423.
3. Talreja, D., P.K. Singh, and A. Kumar, *In Vivo Role of TLR2 and MyD88 Signaling in Eliciting Innate Immune Responses in Staphylococcal Endophthalmitis.* Invest Ophthalmol Vis Sci, 2015. **56**(3): p. 1719-32.
4. Durand, M.L., *Endophthalmitis.* Clin Microbiol Infect, 2013. **19**(3): p. 227-34.
5. Livingston, E.T., M.H. Mursalin, and M.C. Callegan, *A Pyrrhic Victory: The PMN Response to Ocular Bacterial Infections.* Microorganisms, 2019. **7**(11).
6. Miller, F.C., et al., *Targets of immunomodulation in bacterial endophthalmitis.* Prog Retin Eye Res, 2019. **73**: p. 100763.
7. Shamsuddin, N. and A. Kumar, *TLR2 mediates the innate response of retinal Muller glia to Staphylococcus aureus.* J Immunol, 2011. **186**(12): p. 7089-97.
8. Metrikin, D.C., et al., *Measurement of blood-retinal barrier breakdown in endotoxin-induced endophthalmitis.* Invest Ophthalmol Vis Sci, 1995. **36**(7): p. 1361-70.
9. Coburn, P.S., et al., *Blood-Retinal Barrier Compromise and Endogenous Staphylococcus aureus Endophthalmitis.* Invest Ophthalmol Vis Sci, 2015. **56**(12): p. 7303-11.

10. Singh, S., S. Singh, and A. Kumar, *Systemic Candida albicans Infection in Mice Causes Endogenous Endophthalmitis via Breaching the Outer Blood-Retinal Barrier.* Microbiol Spectr, 2022. **10**(4): p. e0165822.
11. Conrady, C.D., et al., *Long-term visual outcomes of endophthalmitis and the role of systemic steroids in addition to intravitreal dexamethasone.* BMC Ophthalmology, 2020. **20**(1): p. 181.
12. Pershing, S., et al., *Endophthalmitis after Cataract Surgery in the United States: A Report from the Intelligent Research in Sight Registry, 2013–2017.* Ophthalmology, 2020. **127**(2): p. 151-158.
13. Shivaramaiah, H.S., et al., *Endophthalmitis caused by gram-positive bacteria resistant to vancomycin: Clinical settings, causative organisms, antimicrobial susceptibilities, and treatment outcomes.* Am J Ophthalmol Case Rep, 2018. **10**: p. 211-214.
14. Antimicrobial Resistance, C., *Global burden of bacterial antimicrobial resistance in 2019: a systematic analysis.* Lancet, 2022. **399**(10325): p. 629-655.
15. Rajamani, D., et al., *Temporal retinal transcriptome and systems biology analysis identifies key pathways and hub genes in Staphylococcus aureus endophthalmitis.* Sci Rep, 2016. **6**: p. 21502.
16. Singh, S., et al., *Integrative metabolomics and transcriptomics identifies itaconate as an adjunct therapy to treat ocular bacterial infection.* Cell Rep Med, 2021. **2**(5): p. 100277.
17. Singh, S., P.K. Singh, and A. Kumar, *Butyrate Ameliorates Intraocular Bacterial Infection by Promoting Autophagy and Attenuating the Inflammatory Response.* Infect Immun, 2023. **91**(1): p. e0025222.
18. Francis, R., et al., *Glycolytic inhibitor 2-deoxyglucose suppresses inflammatory response in innate immune cells and experimental staphylococcal endophthalmitis.* Exp Eye Res, 2020. **197**: p. 108079.
19. Hardie, D.G., *AMP-activated protein kinase: an energy sensor that regulates all aspects of cell function.* Genes Dev, 2011. **25**(18): p. 1895-908.
20. Pokhrel, R.H., et al., *AMPK promotes antitumor immunity by downregulating PD-1 in regulatory T cells via the HMGCR/p38 signaling pathway.* Mol Cancer, 2021. **20**(1): p. 133.
21. Pokhrel, R.H., et al., *AMPK Amplifies IL2-STAT5 Signaling to Maintain Stability of Regulatory T Cells in Aged Mice.* Int J Mol Sci, 2022. **23**(20).
22. Rao, E., et al., *AMPK-dependent and independent effects of AICAR and compound C on T-cell responses.* Oncotarget, 2016. **7**(23): p. 33783-95.
23. Herzig, S. and R.J. Shaw, *AMPK: guardian of metabolism and mitochondrial homeostasis.* Nat Rev Mol Cell Biol, 2018. **19**(2): p. 121-135.
24. Trefts, E. and R.J. Shaw, *AMPK: restoring metabolic homeostasis over space and time.* Mol Cell, 2021. **81**(18): p. 3677-3690.
25. Singh, P.K., D.M. Donovan, and A. Kumar, *Intravitreal injection of the chimeric phage endolysin Ply187 protects mice from Staphylococcus aureus endophthalmitis.* Antimicrob Agents Chemother, 2014. **58**(8): p. 4621-9.
26. Das, S., S. Singh, and A. Kumar, *Bacterial Burden Declines But Neutrophil Infiltration and Ocular Tissue Damage Persist in Experimental Staphylococcus epidermidis Endophthalmitis.* Front Cell Infect Microbiol, 2021. **11**: p. 780648.
27. Swamydas, M. and M.S. Lionakis, *Isolation, purification and labeling of mouse bone marrow neutrophils for functional studies and adoptive transfer experiments.* J Vis Exp, 2013(77): p. e50586.
28. Livak, K.J. and T.D. Schmittgen, *Analysis of relative gene expression data using real-time quantitative PCR and the 2(-Delta Delta C(T)) Method.* Methods, 2001. **25**(4): p. 402-8.
29. Peake, K., et al., *Busulfan as a myelosuppressive agent for generating stable high-level bone marrow chimerism in mice.* J Vis Exp, 2015(98): p. e52553.

30. Durand, M.L., *Bacterial and Fungal Endophthalmitis.* Clin Microbiol Rev, 2017. **30**(3): p. 597-613.
31. van Langevelde, P., et al., *Antibiotic-induced lipopolysaccharide (LPS) release from Salmonella typhi: delay between killing by ceftazidime and imipenem and release of LPS.* Antimicrob Agents Chemother, 1998. **42**(4): p. 739-43.
32. van Langevelde, P., et al., *Antibiotic-Induced Release of Lipoteichoic Acid and Peptidoglycan from Staphylococcus aureus: Quantitative Measurements and Biological Reactivities.* Antimicrobial Agents and Chemotherapy, 1998. **42**(12): p. 3073-3078.
33. Heumann, D., et al., *Gram-positive cell walls stimulate synthesis of tumor necrosis factor alpha and interleukin-6 by human monocytes.* Infect Immun, 1994. **62**(7): p. 2715-21.
34. Bui, D.K. and P.E. Carvounis, *Evidence for and against intravitreous corticosteroids in addition to intravitreous antibiotics for acute endophthalmitis.* Int Ophthalmol Clin, 2014. **54**(2): p. 215-24.
35. Sadaka, A., M.L. Durand, and M.S. Gilmore, *Bacterial endophthalmitis in the age of outpatient intravitreal therapies and cataract surgeries: Host-microbe interactions in intraocular infection.* Prog Retin Eye Res, 2012. **31**(4): p. 316-31.
36. Albrecht, E., et al., *Adjunctive use of intravitreal dexamethasone in presumed bacterial endophthalmitis: a randomised trial.* British Journal of Ophthalmology, 2011. **95**(10): p. 1385-1388.
37. Shah, G.K., et al., *Visual outcomes following the use of intravitreal steroids in the treatment of postoperative endophthalmitis.* Ophthalmology, 2000. **107**(3): p. 486-9.
38. Renfro, L. and J.S. Snow, *Ocular effects of topical and systemic steroids.* Dermatol Clin, 1992. **10**(3): p. 505-12.
39. Wiskur, B.J., et al., *Toward improving therapeutic regimens for Bacillus endophthalmitis.* Invest Ophthalmol Vis Sci, 2008. **49**(4): p. 1480-7.
40. Meredith, T.A., et al., *Intraocular dexamethasone produces a harmful effect on treatment of experimental Staphylococcus aureus endophthalmitis.* Trans Am Ophthalmol Soc, 1996. **94**: p. 241-52; discussion 252-7.
41. Schulman, J.A. and G.A. Peyman, *Intravitreal corticosteroids as an adjunct in the treatment of bacterial and fungal endophthalmitis. A review.* Retina, 1992. **12**(4): p. 336-40.
42. Baum, J.L., et al., *The effect of corticosteroids in the treatment of experimental bacterial endophthalmitis.* Am J Ophthalmol, 1975. **80**(3 Pt 2): p. 513-5.
43. Liu, S.M., et al., *Effects of intravitreal corticosteroids in the treatment of Bacillus cereus endophthalmitis.* Arch Ophthalmol, 2000. **118**(6): p. 803-6.
44. Al Dhibi, H.A. and J.F. Arevalo, *Clinical trials on corticosteroids for diabetic macular edema.* World J Diabetes, 2013. **4**(6): p. 295-302.
45. Hawley, S.A., et al., *Complexes between the LKB1 tumor suppressor, STRAD alpha/beta and MO25 alpha/beta are upstream kinases in the AMP-activated protein kinase cascade.* J Biol, 2003. **2**(4): p. 28.
46. Woods, A., et al., *LKB1 is the upstream kinase in the AMP-activated protein kinase cascade.* Curr Biol, 2003. **13**(22): p. 2004-8.
47. Woods, A., et al., *Ca2+/calmodulin-dependent protein kinase kinase-beta acts upstream of AMP-activated protein kinase in mammalian cells.* Cell Metab, 2005. **2**(1): p. 21-33.
48. Hurley, R.L., et al., *The Ca2+/calmodulin-dependent protein kinase kinases are AMP-activated protein kinase kinases.* J Biol Chem, 2005. **280**(32): p. 29060-6.
49. Hawley, S.A., et al., *Calmodulin-dependent protein kinase kinase-beta is an alternative upstream kinase for AMP-activated protein kinase.* Cell Metab, 2005. **2**(1): p. 9-19.
50. Sato, S., et al., *Essential function for the kinase TAK1 in innate and adaptive immune responses.* Nat Immunol, 2005. **6**(11): p. 1087-95.

51. Mangalam, A.K., et al., *AMP-Activated Protein Kinase Suppresses Autoimmune Central Nervous System Disease by Regulating M1-Type Macrophage-Th17 Axis.* J Immunol, 2016. **197**(3): p. 747-60.
52. Nieves, W., et al., *Myeloid-Restricted AMPKalpha1 Promotes Host Immunity and Protects against IL-12/23p40-Dependent Lung Injury during Hookworm Infection.* J Immunol, 2016. **196**(11): p. 4632-40.
53. Mounier, R., et al., *AMPKalpha1 regulates macrophage skewing at the time of resolution of inflammation during skeletal muscle regeneration.* Cell Metab, 2013. **18**(2): p. 251-64.
54. Wang, S., et al., *Role of AMPK in autophagy.* Front Physiol, 2022. **13**: p. 1015500.
55. Bae, H.B., et al., *AMP-activated protein kinase enhances the phagocytic ability of macrophages and neutrophils.* FASEB J, 2011. **25**(12): p. 4358-68.
56. Kajiwara, C., et al., *Metformin Mediates Protection against Legionella Pneumonia through Activation of AMPK and Mitochondrial Reactive Oxygen Species.* J Immunol, 2018. **200**(2): p. 623-631.
57. Becker, E., et al., *AMPK activation improves recovery from pneumonia-induced lung injury via reduction of er-stress and apoptosis in alveolar epithelial cells.* Respiratory Research, 2023. **24**(1): p. 185.
58. Singh, S., et al., *AMP-Activated Protein Kinase Restricts Zika Virus Replication in Endothelial Cells by Potentiating Innate Antiviral Responses and Inhibiting Glycolysis.* J Immunol, 2020. **204**(7): p. 1810-1824.
59. Silwal, P., et al., *AMP-Activated Protein Kinase and Host Defense against Infection.* Int J Mol Sci, 2018. **19**(11).
60. Rosenberg, G., et al., *Immunometabolic crosstalk during bacterial infection.* Nat Microbiol, 2022. **7**(4): p. 497-507.
61. Urso, A. and A. Prince, *Anti-Inflammatory Metabolites in the Pathogenesis of Bacterial Infection.* Front Cell Infect Microbiol, 2022. **12**: p. 925746.
62. Khan, A., et al., *Macrophage heterogeneity and plasticity in tuberculosis.* J Leukoc Biol, 2019. **106**(2): p. 275-282.
63. Wynn, T.A. and K.M. Vannella, *Macrophages in Tissue Repair, Regeneration, and Fibrosis.* Immunity, 2016. **44**(3): p. 450-462.
64. Castro-Dopico, T., et al., *GM-CSF Calibrates Macrophage Defense and Wound Healing Programs during Intestinal Infection and Inflammation.* Cell Rep, 2020. **32**(1): p. 107857.

Figure Legends

Fig. 1: Myeloid-specific AMPKα1 deficiency exacerbates endophthalmitis severity in mice. (A-B) Endophthalmitis was induced in AMPKα1^{fl} (Wt mice) or LysM^{Cre};α1^{fl} (myeloid-specific AMPKα1 deficient) n = 6 per time point: 24, 48, and 72 h) by intravitreal inoculation of *S. aureus* RN6390 (5,00 CFUs/eye). Eyes injected with PBS were used as controls. Representative slit-lamp micrograph showing corneal haze/opacity and H&E staining of enucleated eyes showing retinal damage and immune cell infiltration. C, cornea; AC, anterior chamber; L, lens; VC, vitreous chamber; R, retina. **(C)** Scotopic ERG response as measured by the percentage of a-and b-wave amplitudes retained in comparison to uninfected control eyes with values maintained at 100%. **(D)** Quantitation of intraocular bacterial burden by serial dilution and plate count represented as CFUs/eye (n=6). **(E)** Corneal opacity was measured using ImageJ and is represented as the integrated pixel intensity. The data represent the culmination of two independent experiments and are shown as the mean ± SD. Statistical analysis was performed using one-way ANOVA with Tukey's multiple comparisons test (panels C, D, & E). ns = not significant*; *P< 0.01; **P< 0.001; ***P< 0.0001.*

Fig. 2: Myeloid cell-specific AMPKα1 deletion enhances inflammation in *S. aureus*-infected eyes. (A-B) Endophthalmitis was induced in AMPKα1^{fl} (WT mice) or

622 LysM^{Cre}; AMPKα1^{fl} (n = 6 per time point: 24, 48, and 72 h) by intravitreal inoculation of
623 *S. aureus* RN6390 (5,00 CFUs/eye). Eyes injected with PBS were used as controls. At
624 the indicated time points, the eyes or retinas were harvested, and ELISA or qPCR was
625 performed to measure the levels of the indicated inflammatory cytokines or chemokines
626 in whole eye lysates or retinas (n = 6). The data represent the culmination of two
627 independent experiments and are shown as the mean ± SD. Statistical analysis was
628 performed using one-way ANOVA with Tukey's multiple comparisons test (panels A &
629 B). ns = not significant*; *P< 0.01; **P< 0.001; ***P< 0.0001.*

630 **Fig. 3: *S. aureus*-infected BMDMs lacking AMPKα1 exhibit a distinct**
631 **transcriptomic signature profile and attenuated phagocytosis.** BMDMs from WT or
632 AMPKα1 knock-out (KO) mice were infected with *S. aureus* (MOI 10:1) for 6 h
633 (n=3/condition). RNA was extracted, and RNA sequencing was performed using the
634 Illumina platform. **(A)** Volcano plot showing the overall distribution of differentially
635 expressed genes (DEGs). The points represent genes, blue dots indicate no significant
636 difference in genes, red dots indicate upregulated differentially expressed genes, and
637 green dots indicate downregulated differentially expressed genes. The Y-axis shows the
638 adjusted p-value ($\log_{10}$) and the X-axis shows the $\log_2$ fold change. **(B)** Gene Ontology
639 enrichment analysis shows the significantly enriched downregulated pathways in KO
640 BMDMs compared to the Wt BMDMs. **(C)** Bubble plot showing enrichment scores for
641 downregulated pathways in KO BMDMs. The size of the sphere is based on the positive
642 enrichment score. **(D)** Heatmap showing DEGs in *S. aureus* (SA)-infected KO vs WT
643 BMDMs.

Fig. 4: AMPKα1 deficiency promotes M1 macrophage phenotypes in *S. aureus*-infected eyes and BMDMs. (A-B) Endophthalmitis was induced in AMPKα1^{fl} or LysM^{Cre}; AMPKα1^{fl} (n = 6 per time point: 24, 48, and 72 h) by intravitreal inoculation of *S. aureus* RN6390 (500 CFUs/eye). Eyes injected with PBS were used as controls. At the indicated time points, the retinas were harvested, and qPCR was performed to measure the expression profiles of M1 and M2 macrophage phenotype markers (n=6). **(C-D)** BMDMs from AMPKα1^{fl} (WT mice) or LysM^{Cre}; AMPKα1^{fl} (AMPKα1 deficient) mice were infected with *S. aureus* (MOI 10:1) for immunostaining (3 h). Immunostaining was performed for iNOS (red) or Arg1 (Green) expression and images were captured at the original magnification of 60X. **(E-F & G-H)** BMDMs from AMPKα1^{fl} (WT mice) or LysM^{Cre}; AMPKα1^{fl} mice were infected with *S. aureus* (MOI 10:1) for western blotting (3 h). Western blot was performed to detect iNOS, Arg1, and HSP90 proteins. Densitometry analysis was performed using ImageJ and data are expressed as relative fold changes normalized to the loading control, HSP90. The data are representative of two independent experiments and are shown as the mean ± SD. Statistical analysis was performed using one-way ANOVA with Tukey's multiple comparisons test (panels A & B, E & G). ns = not significant; *P< 0.01; **P< 0.001; ***P< 0.0001.

Fig. 5: *Adoptive transfer of wild-type myeloid cells to AMPKα1 deficient mice rescues S. aureus-induced endophthalmitis.* (A) Schematic of experimental design for bone marrow transplant and endophthalmitis. **(B-C)** Endophthalmitis was induced in AMPKα1 KO (recipient), and B6.SJL-*Ptprc*^{a} *Pepc*^{b}/BoyJ (PepBoy, donor) (B6 background, n = 4, time point: 72 h) by intravitreal inoculation of *S. aureus* RN6390 (5,00 CFUs/eye). Eyes injected with PBS were used as controls. Representative slit-

lamp micrograph showing corneal haze/opacity. **(C)** Scotopic ERG response as measured by the percentage of a-and b-wave amplitudes retained in comparison to uninfected control eyes with values kept at 100%. **(D)** Corneal opacity was measured using ImageJ and represented as integrated pixel intensity. **(E)** Quantitation of intraocular bacterial burden by serial dilution and plate count represented as CFUs/eye (n=4). **(F & G)** At the indicated time points, the eyes or retinas were harvested and ELISA or flow cytometry was performed to measure the levels of inflammatory cytokines or chemokines from whole eye lysates or neutrophile infiltration from the retinas (n=4). **(H)** Bar graph showing the frequency of neutrophil infiltration in chimeric mice. The data represented are the culmination of two independent experiments and are shown as the mean ± SD. Statistical analysis was performed using one-way ANOVA with Tukey's multiple comparisons (panels B, & E) or unpaired t-test (C & D). ns = not significant*; *P< 0.01; **P< 0.001; ***P< 0.0001.*

Fig. 6. **Effect of myeloid cell-specific AMPKα1 deletion on *S. aureus*-induced endophthalmitis.** Mechanistically, myeloid-specific AMPKα1 inactivation impairs the phagocytic clearance of *S. aureus* and the resolution of inflammation by skewing toward the M1 macrophage phenotype. The adoptive transfer of AMPK-competent bone marrow from WT mice to AMPKα1 deficient mice preserved retinal functions and attenuated disease severity.

Supplementary Figures.

Fig. S1: *Myeloid cell-specific AMPKα1 loss* enhances the inflammation in *S. aureus*-infected BMDMs. BMDMs from AMPKα1^{fl} or LysM^{Cre}; AMPKα1^{fl} (n=4/condition) were infected with *S. aureus* (MOI 10:1) for 6h. The expression of inflammatory cytokines was measured by **(A)** qPCR and **(B)** ELISA. The data represent the culmination of two independent experiments and are shown as the mean ± SD. Statistical analysis was performed using one-way ANOVA with Tukey's multiple comparisons test (panels A & B). ns = not significant*; *P< 0.01; **P< 0.001; ***P< 0.0001.*

Fig. S2: AMPKα deficient BMDMs exhibit attenuation of antimicrobial gene expression and phagocytosis. (A) BMDMs from AMPKα1^{fl} or LysM^{Cre}; AMPKα1^{fl} (n=4/condition) were infected with *S. aureus* (MOI 10:1) for 6 h. The expression profiles of genes (e.g., *S100a7, S100a8,* and *S100a10*) with antimicrobial functions were assessed by qPCR. **(B)** BMDMs from AMPKα1^{fl} or LysM^{Cre}; AMPKα1^{fl} (n=4/condition) were challenged with *S. aureus* (MOI 10:1) for 2 h. After 2 h of infection, the cells were rinsed to remove extracellular bacteria and incubated with fresh medium containing

712 gentamicin (200 μg/mL) for the indicated time points. At the desired time point, the cells
713 were lysed, and the viable bacterial counts were quantitated via serial dilution and
714 counting. Statistical analysis was performed using one-way ANOVA with Tukey's
715 multiple comparison test (panels A, & B). The data represents mean ± SD from three
716 independent experiments. ns = not significant; $^{**}P < 0.01$; $^{**}P < 0.001$.

Fig 1

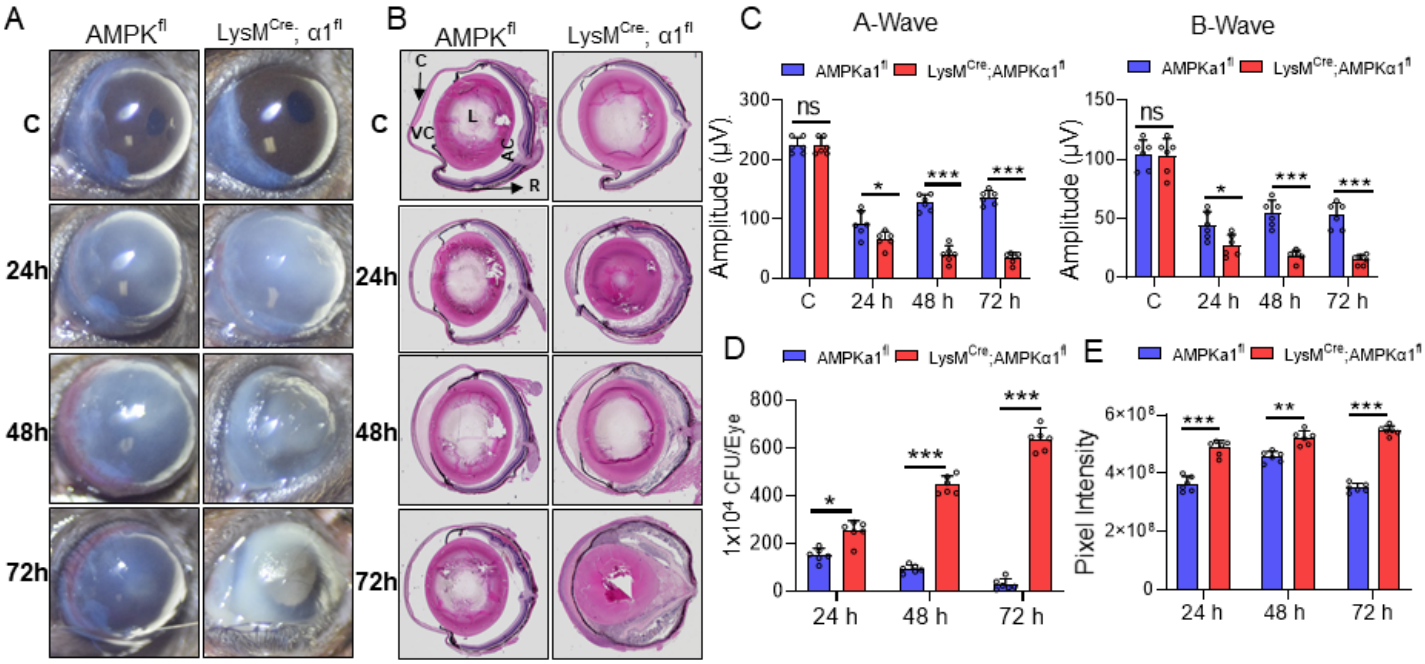
A
AMPK^fl
LysM^Cre; α1^fl
C
24h
48h
72h
B
AMPK^fl
LysM^Cre; α1^fl
C
VC
L
AC
R
C
24h
48h
72h
C
A-Wave
B-Wave
AMPKa1^fl
LysM^Cre;AMPKα1^fl
Amplitude (μV)
ns
*
***
C
24 h
48 h
72 h
D
1x10⁴ CFU/Eye
E
Pixel Intensity
**

Fig 2

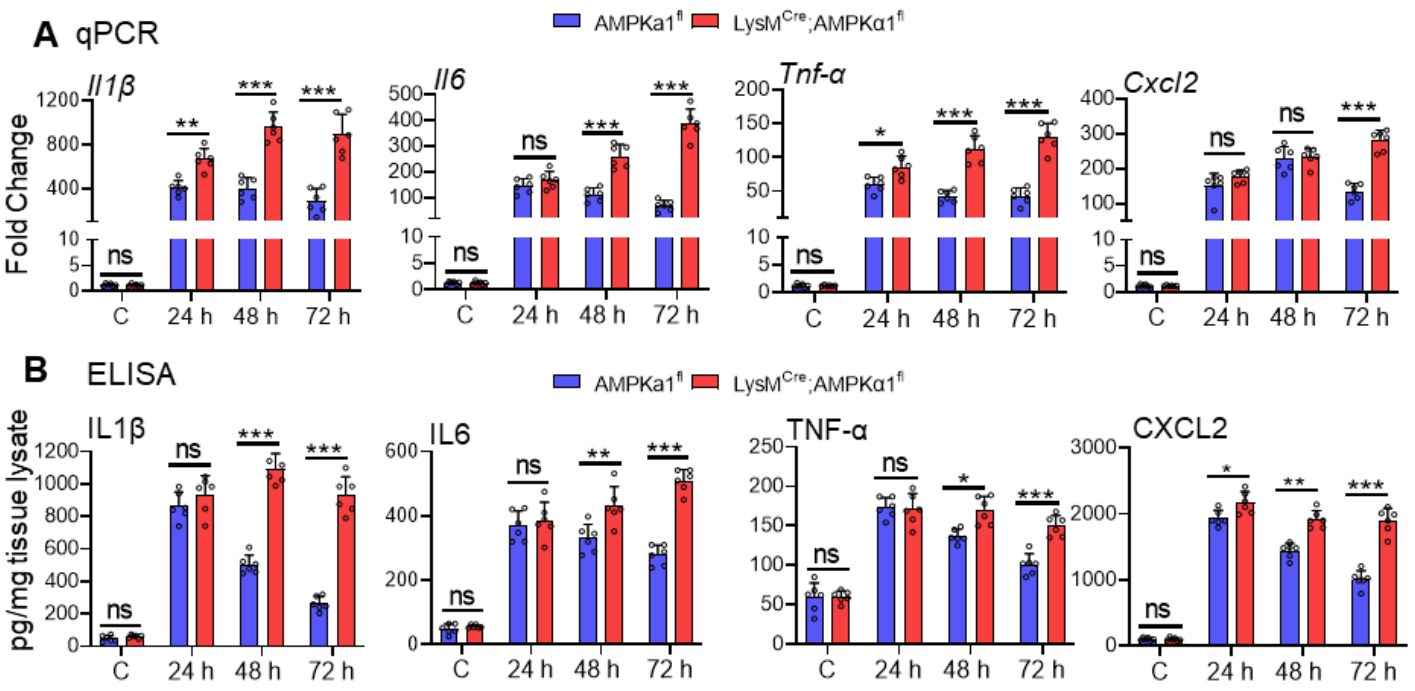
A qPCR
AMPKa1fl
LysMCre;AMPKα1fl
Il1β
Il6
Tnf-α
Cxcl2
Fold Change
ns
C
24 h
48 h
72 h
B ELISA
IL1β
IL6
TNF-α
CXCL2
pg/mg tissue lysate

Fig 3

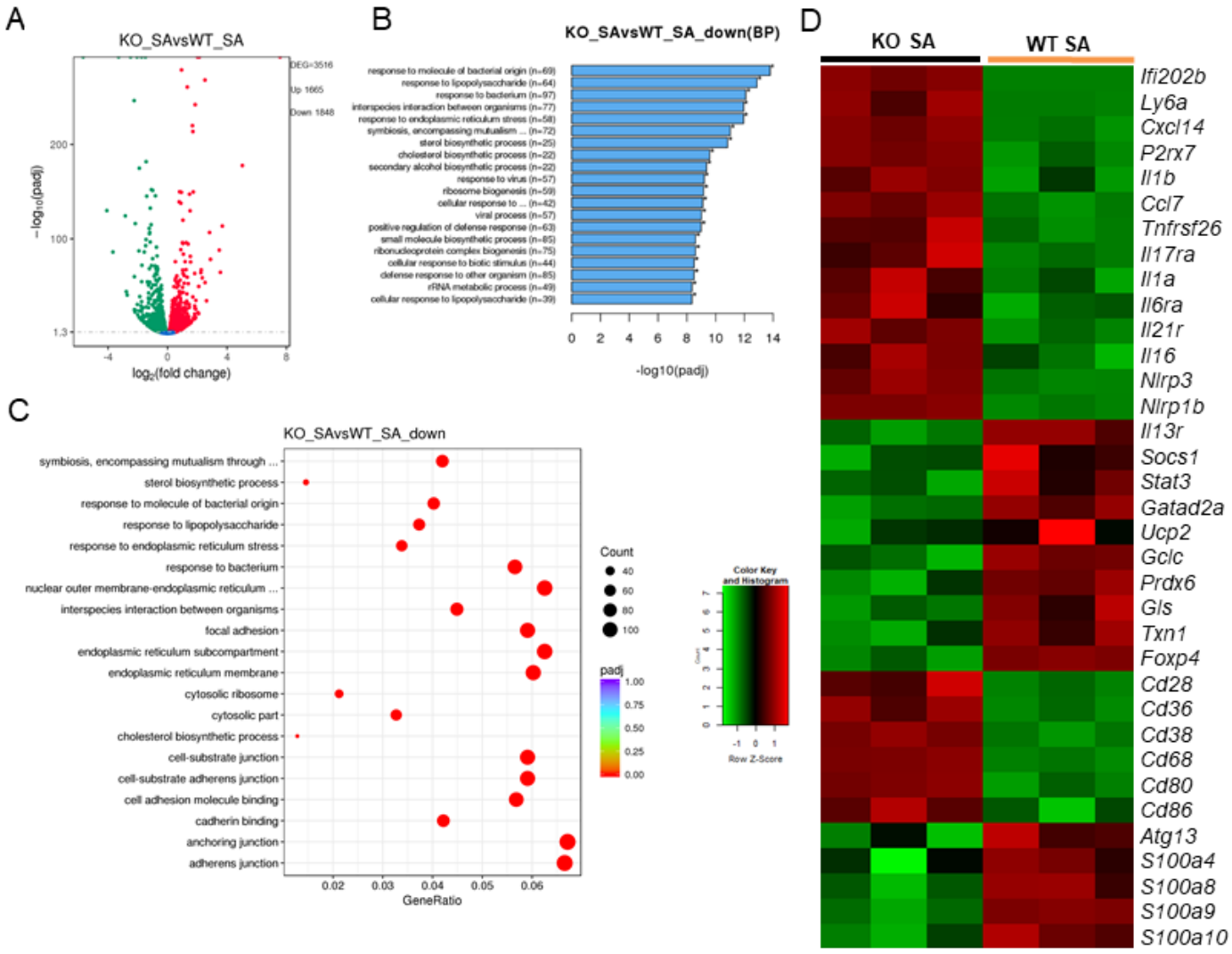
A
KO_SAvsWT_SA
DEG=3516
Up 1665
Down 1848
B
KO_SAvsWT_SA_down(BP)
response to molecule of bacterial origin (n=69)
response to lipopolysaccharide (n=64)
response to bacterium (n=97)
interspecies interaction between organisms (n=77)
response to endoplasmic reticulum stress (n=58)
symbiosis, encompassing mutualism ... (n=72)
sterol biosynthetic process (n=25)
cholesterol biosynthetic process (n=22)
secondary alcohol biosynthetic process (n=22)
response to virus (n=57)
ribosome biogenesis (n=59)
cellular response to ... (n=42)
viral process (n=57)
positive regulation of defense response (n=63)
small molecule biosynthetic process (n=85)
ribonucleoprotein complex biogenesis (n=75)
cellular response to biotic stimulus (n=44)
defense response to other organism (n=85)
rRNA metabolic process (n=49)
cellular response to lipopolysaccharide (n=39)
-log10(padj)
C
KO_SAvsWT_SA_down
symbiosis, encompassing mutualism through ...
sterol biosynthetic process
response to molecule of bacterial origin
response to lipopolysaccharide
response to endoplasmic reticulum stress
response to bacterium
nuclear outer membrane-endoplasmic reticulum ...
interspecies interaction between organisms
focal adhesion
endoplasmic reticulum subcompartment
endoplasmic reticulum membrane
cytosolic ribosome
cytosolic part
cholesterol biosynthetic process
cell-substrate junction
cell-substrate adherens junction
cell adhesion molecule binding
cadherin binding
anchoring junction
adherens junction
GeneRatio
Count
padj
Color Key and Histogram
Row Z-Score
D
KO SA
WT SA
Ifi202b
Ly6a
Cxcl14
P2rx7
Il1b
Ccl7
Tnfrsf26
Il17ra
Il1a
Il6ra
Il21r
Il16
Nlrp3
Nlrp1b
Il13r
Socs1
Stat3
Gatad2a
Ucp2
Gclc
Prdx6
Gls
Txn1
Foxp4
Cd28
Cd36
Cd38
Cd68
Cd80
Cd86
Atg13
S100a4
S100a8
S100a9
S100a10

Fig 4

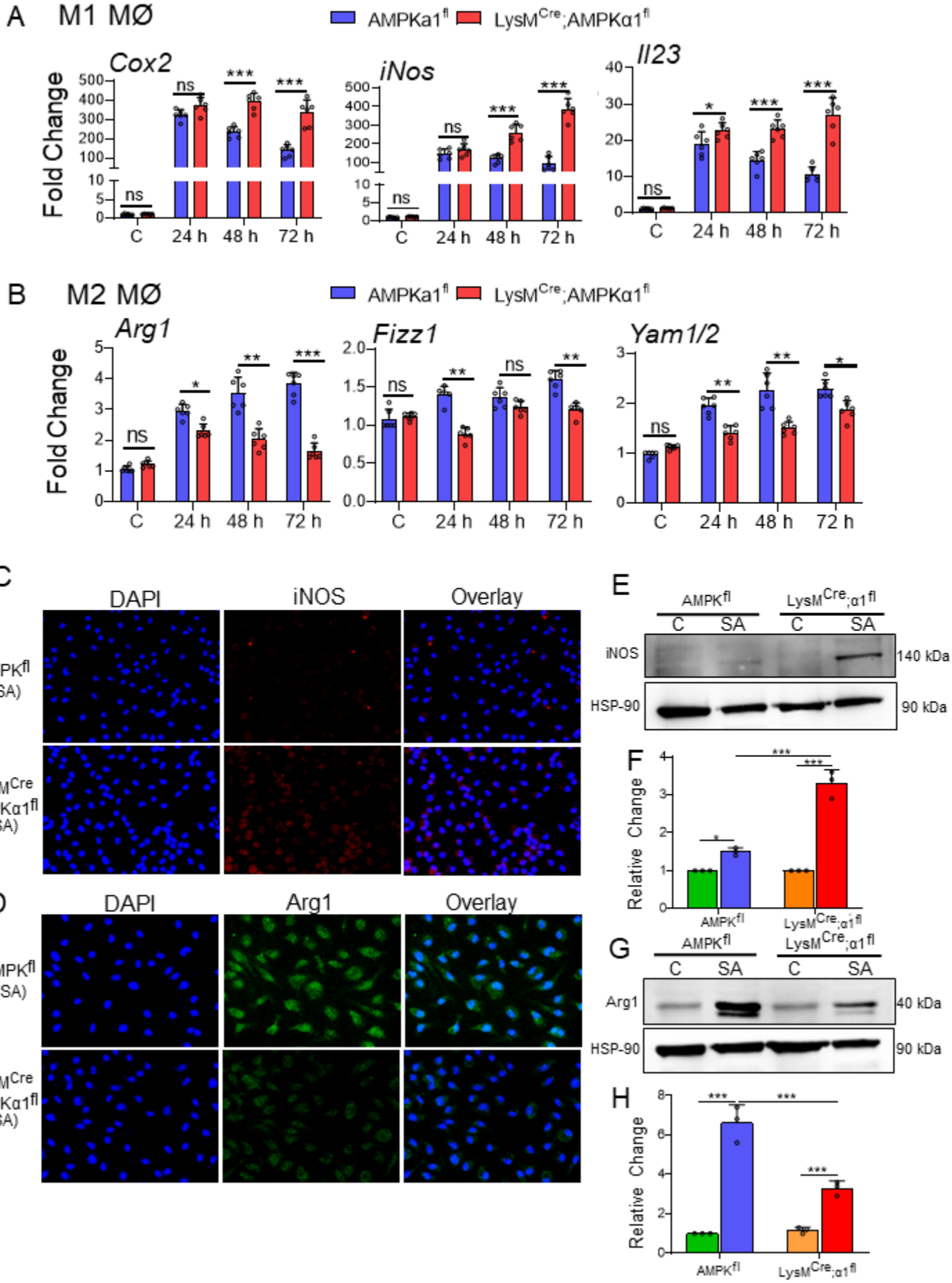
A M1 MØ
AMPKa1fl LysMCre;AMPKα1fl
Cox2
iNos
Il23
Fold Change
C 24 h 48 h 72 h
B M2 MØ
Arg1
Fizz1
Yam1/2
C
DAPI iNOS Overlay
AMPKfl (SA)
LysMCre AMPKα1fl (SA)
D
DAPI Arg1 Overlay
E
AMPKfl LysMCre;α1fl
C SA C SA
iNOS
HSP-90
140 kDa
90 kDa
F
Relative Change
G
Arg1
40 kDa
H

Fig 5

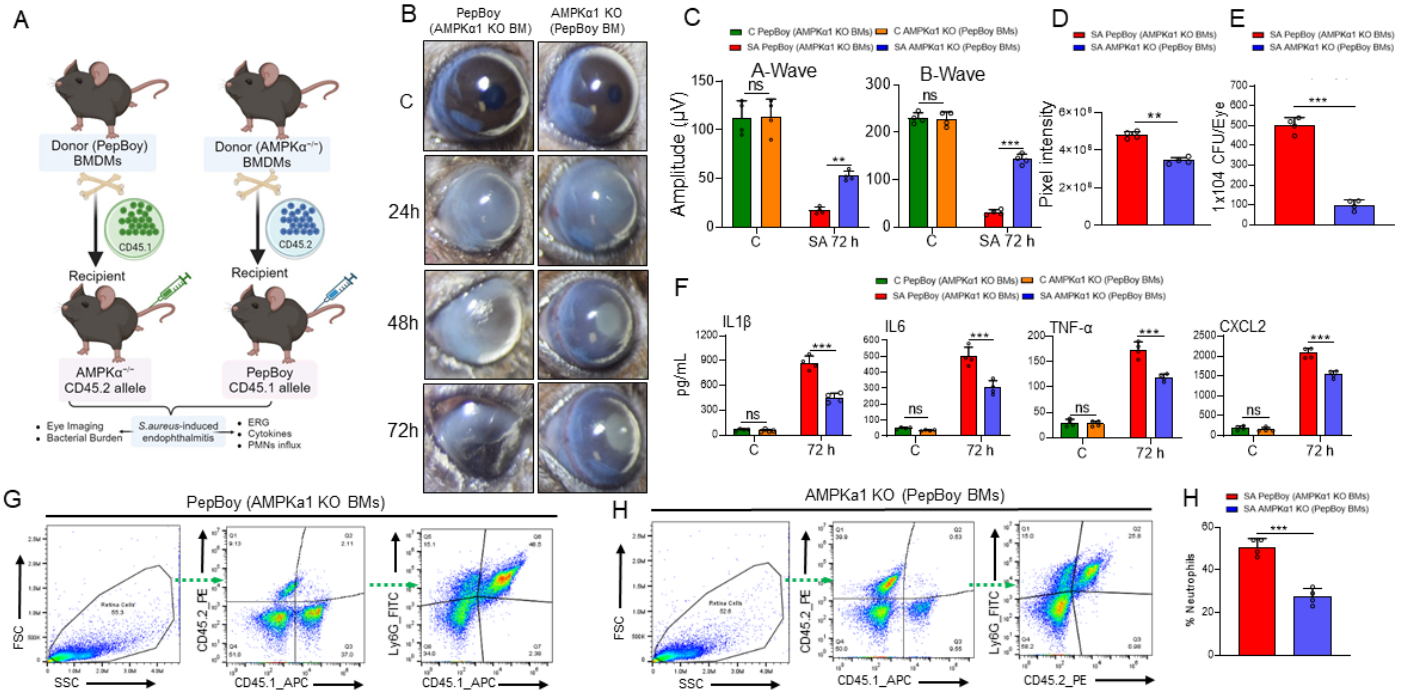
A
Donor (PepBoy) BMDMs
Donor (AMPKα⁻/⁻) BMDMs
CD45.1
CD45.2
Recipient
Recipient
AMPKα⁻/⁻ CD45.2 allele
PepBoy CD45.1 allele
Eye Imaging
Bacterial Burden
S.aureus-induced endophthalmitis
ERG
Cytokines
PMNs influx
B
PepBoy (AMPKα1 KO BM)
AMPKα1 KO (PepBoy BM)
C
24h
48h
72h
C
C PepBoy (AMPKα1 KO BMs)
C AMPKα1 KO (PepBoy BMs)
SA PepBoy (AMPKα1 KO BMs)
SA AMPKα1 KO (PepBoy BMs)
A-Wave
B-Wave
Amplitude (μV)
ns
**
***
C
SA 72 h
D
Pixel intensity
E
1x104 CFU/Eye
F
IL1β
IL6
TNF-α
CXCL2
pg/mL
72 h

G
PepBoy (AMPKa1 KO BMs)
FSC
SSC
CD45.2_PE
CD45.1_APC
Ly6G_FITC
H
AMPKa1 KO (PepBoy BMs)
CD45.2_PE
CD45.1_APC
Ly6G_FITC
CD45.2_PE
H
SA PepBoy (AMPKα1 KO BMs)
SA AMPKα1 KO (PepBoy BMs)
% Neutrophils

Fig 6

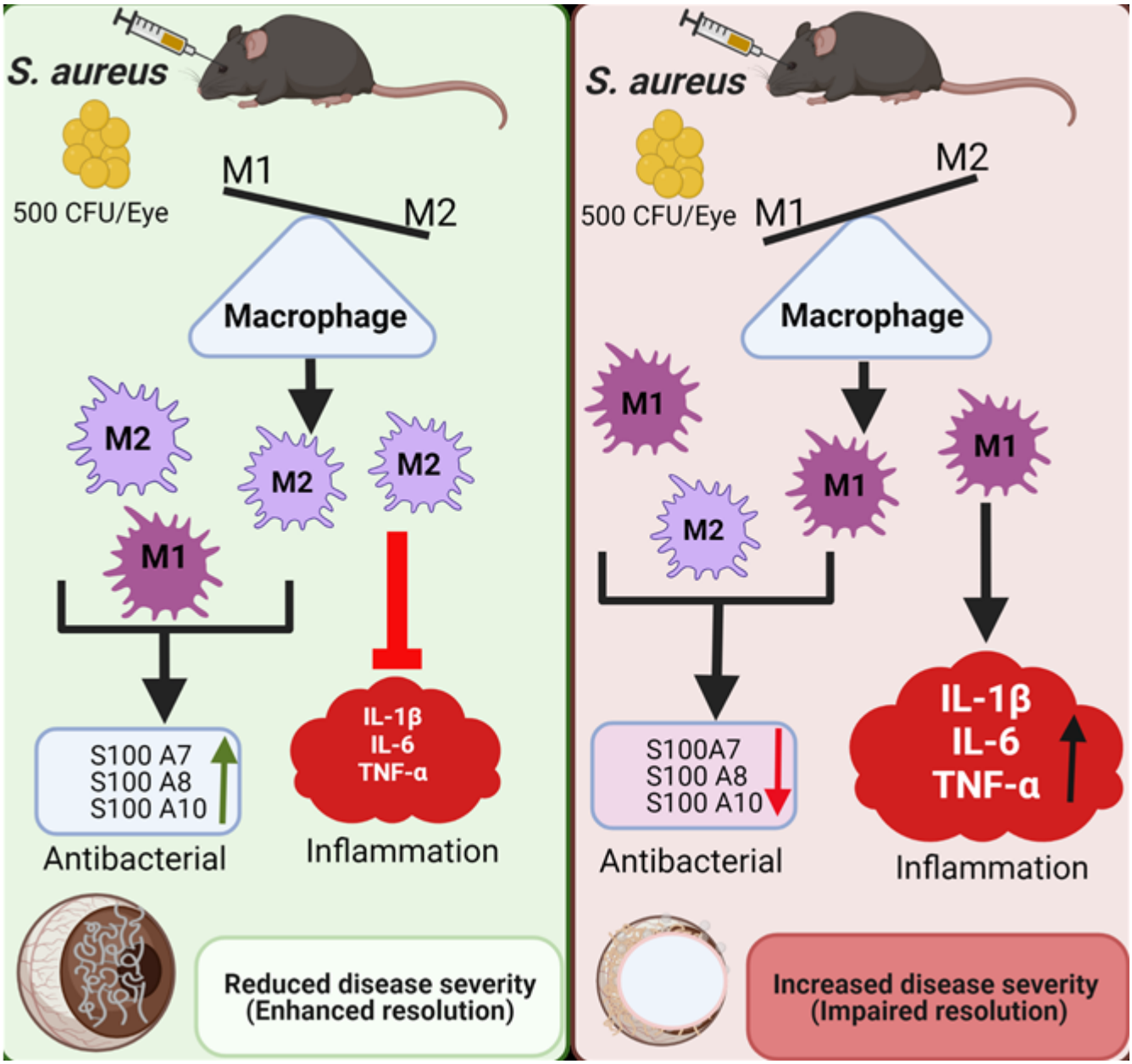
S. aureus
500 CFU/Eye
M1
M2
Macrophage
M2
M2
M2
M1
S100 A7
S100 A8
S100 A10
Antibacterial
IL-1β
IL-6
TNF-α
Inflammation
Reduced disease severity
(Enhanced resolution)
S. aureus
500 CFU/Eye
M2
M1
Macrophage
M1
M1
M1
M2
S100A7
S100 A8
S100 A10
Antibacterial
IL-1β
IL-6
TNF-α
Inflammation
Increased disease severity
(Impaired resolution)

Fig 1S

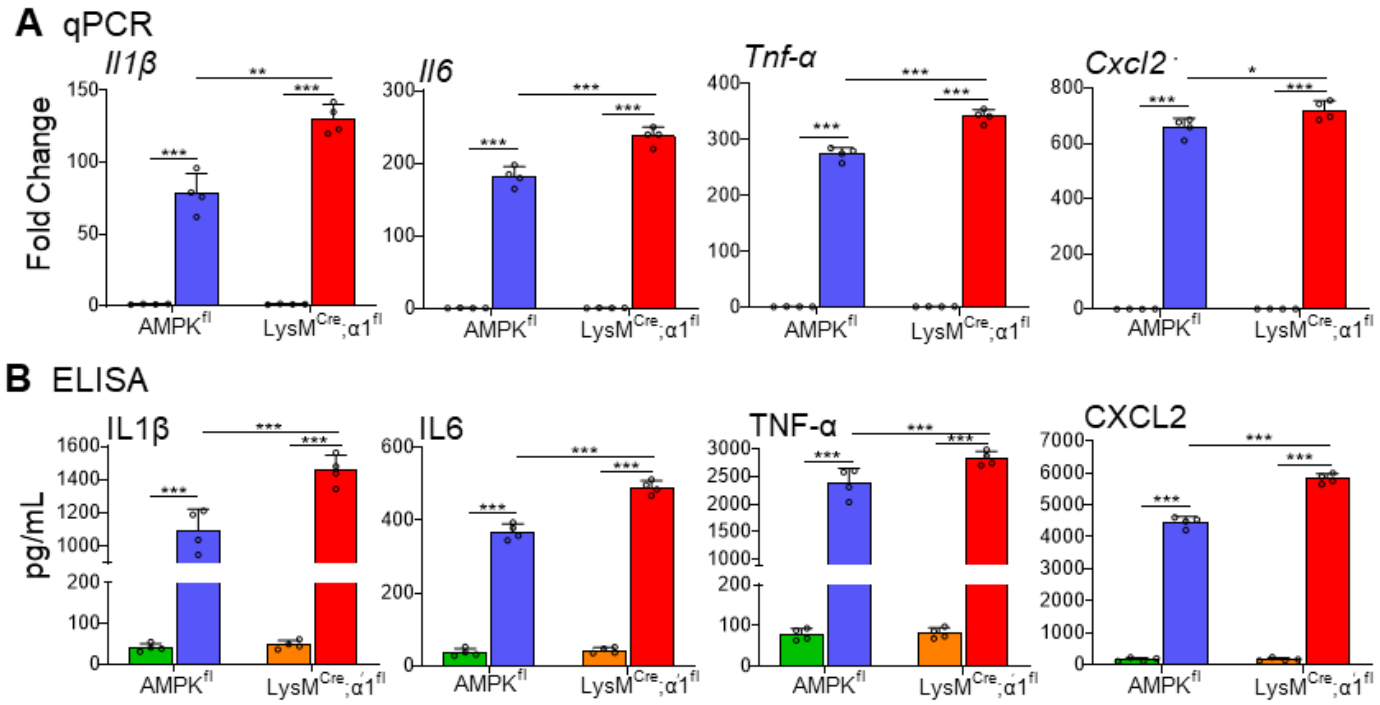
A qPCR
Il1β
Il6
Tnf-α
Cxcl2
Fold Change
AMPKfl
LysMCre;α1fl
B ELISA
IL1β
IL6
TNF-α
CXCL2
pg/mL

Fig 2S

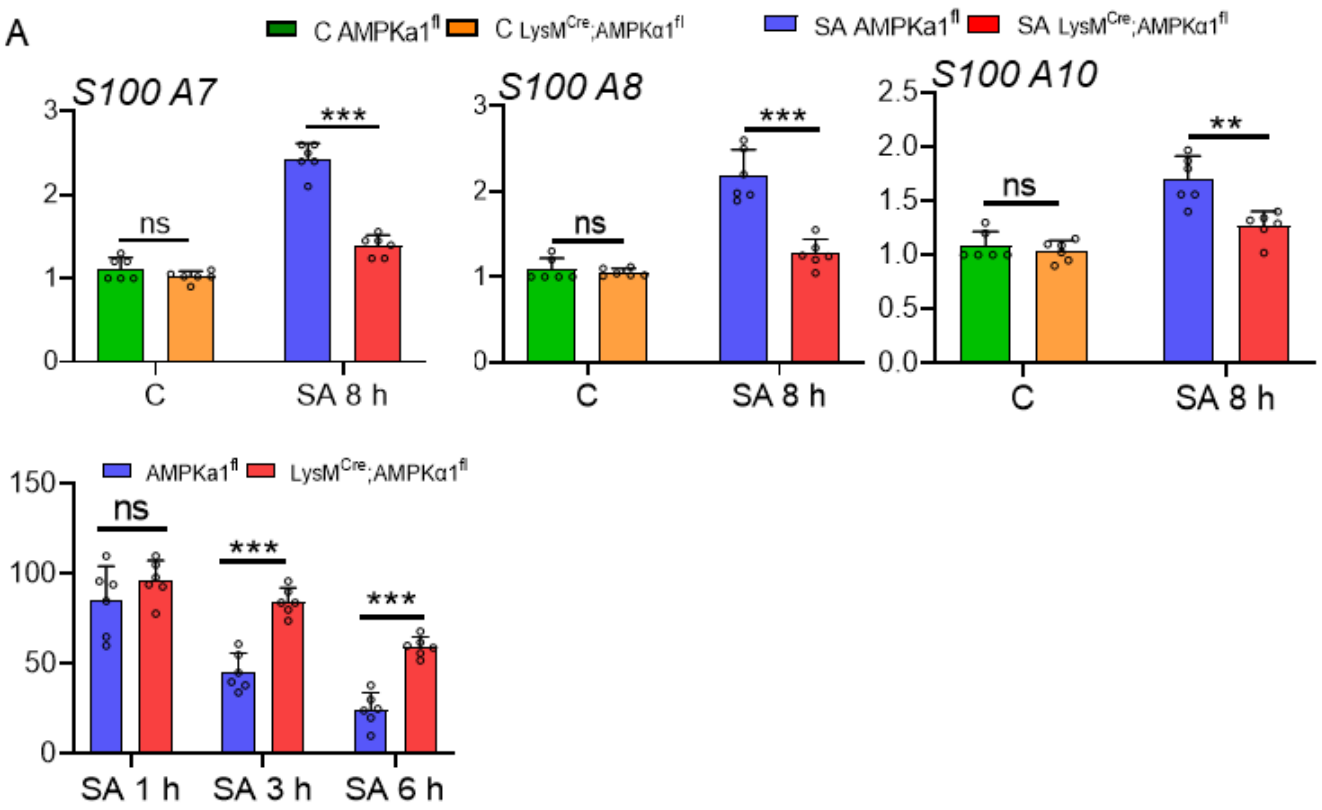
A
C AMPKa1fl
C LysMCre;AMPKα1fl
SA AMPKa1fl
SA LysMCre;AMPKα1fl
S100 A7
S100 A8
S100 A10
ns
***
**
C
SA 8 h
AMPKa1fl
LysMCre;AMPKα1fl
CFU (1^10^4 /mL)
SA 1 h
SA 3 h
SA 6 h